IEEE Access
Multidisciplinary ⋮ Rapid Review ⋮ Open Access Journal

IEEE POWER & ENERGY SOCIETY SECTION

Received 25 November 2024, accepted 15 December 2024, date of publication 20 December 2024, date of current version 30 December 2024.

Digital Object Identifier 10.1109/ACCESS.2024.3520901

RESEARCH ARTICLE

Inertia Estimation and Trend Analysis of the United States Power Grid Interconnections

SAURAV DULAL[1], (Graduate Student Member, IEEE), CHENGWEN ZHANG[1], (Member, IEEE), MOHAMMED OLAMA[2], (Senior Member, IEEE), QIAN LIU[1], (Graduate Student Member, IEEE), NARAYAN BHUSAL[2], (Member, IEEE), AJAY PRATAP YADAV[2], (Member, IEEE), MARK BALDWIN[3], NILS STENVIG[2], (Senior Member, IEEE), AND YILU LIU[1,2], (Life Fellow, IEEE)

[1]Department of Electrical Engineering and Computer Science, University of Tennessee, Knoxville, TN 37996, USA
[2]Oak Ridge National Laboratory, Oak Ridge, TN 37831, USA
[3]Dominion Energy, Glen Allen, VA 23060, USA

Corresponding author: Saurav Dulal (sdulal@vols.utk.edu)

This work was supported by U.S. Department of Energy, Office of Electricity (OE), University of Tennessee (UT)-Battelle, Limited Liability Company (LLC), under Contract DE-AC05-00OR22725.

ABSTRACT The transition from conventional to modern power systems is causing an increase in integration of inverter-based resources (IBRs). This generally leads to a decrease in total system inertia, which in-turn increases the system's rate-of-change-of-frequency (RoCoF) during disturbances. This poses a threat to the frequency stability of the system and may falsely trigger protective devices. To monitor system status and plan for integrating renewable energy sources like photovoltaic, wind, and energy storage systems, a realistic study of inertia estimation and analysis in the United States (US) over the past decade is needed. This paper uses field-measured phasor measurement unit (PMU) data collected throughout the US from 2013 to 2023 via the Frequency Monitoring Network (FNET/GridEye) operated by the University of Tennessee, Knoxville (UTK) and Oak Ridge National Laboratory (ORNL). The collected PMU frequency data is utilized to estimate the system inertia of the three US interconnections: Eastern, Western, and Texas. Various RoCoF time windows are investigated for estimating the inertia of each interconnection by maximizing the correlation coefficient between the measured RoCoF and power mismatch. The resulting inertia trends over the past decade show approximately a 6% decline in inertia in the Eastern interconnection, a 15% decline in inertia in the Western interconnection, and a 16% increase in inertia in Texas. Key insights into how inertia is changing amidst the complex energy landscape are extracted using the fuel mix trend data. This provides valuable information for future energy strategies and planning.

INDEX TERMS Inertia estimation, US interconnections, inverter-based resources (IBRs), rate-of-change-of-frequency (RoCoF), and fuel mix.

I. INTRODUCTION

Synchronous generators (SGs), which dominate the conventional power system network, are now being replaced by inverter-based resources (IBRs). IBRs are renewable energy sources that do not have the spinning mass (rotor) [1], [2]. This lack of rotational energy is causing a decrease in traditionally available inertia. In traditional power systems, inertia is relatively constant, which helps reduce the rate-of-change-of-frequency (RoCoF) and frequency deviation during a power mismatch between load and generation [3]. However, a reduction in system inertia, could lead to an increase in the RoCoF level in case of a contingency. This threatens the frequency stability of the system and may trigger under-frequency relays and other protection control devices [4]. It in-turn may lead to blackouts and cascade tripping as reported in [5] and [6].

Although inertia and RoCoF have been important metrics in the traditional SG-dominated power systems for a long time, they have particularly become pressing issues during

The associate editor coordinating the review of this manuscript and approving it for publication was Nga Nguyen.

the past decade. This is due to the dramatic change of the energy landscape in the United States (US) brought about by the significant increase in generation from renewable sources like photovoltaic (PV) and wind. In addition, there is an increase in generation from gas plants and the corresponding decrease in coal plant production [7]. These shifts underscore the complex energy mix in the power system. Furthermore, the advent of IBRs, which are mostly grid-following in nature and lack natural frequency response capabilities, is making the generation mix more diverse. This diversification has raised critical questions regarding the trend of system inertia. During the last decade these questions have become more significant as the energy mix continues to evolve.

In recent years, several studies have been conducted on the impact of higher integration of IBRs on the grid. Works like [8], [9], [10] have investigated system inertial response under high solar and wind scenarios using various models. The dispatch-based inertia summation methods in [11] and [12] estimate system inertia by summing known generator data, but overlook contributions from IBRs and loads. While modeling approaches like the ARMAX model [13] and the transfer function [14] can effectively extract inertia using frequency and load data, these methods are typically limited to smaller systems. This makes their application to large interconnections challenging. Others studies, such as [15] and [16], have employed a swing equation-based approach to estimate inertia using real event data, but few have fully utilized field-measured data to monitor long-term inertia trends in large systems.

The rise of IBRs has introduced new challenges in inertia estimation, raising questions about the accuracy of traditional models. Wide-area measurement systems (WAMS), which monitor key parameters like frequency, offer valuable insights for more accurate inertia assessment [17], [18]. The utilization of real-event data can address limitations in model-based methods, revealing nuanced system behaviors. Therefore, a comprehensive measurement-based study using phasor measurement unit (PMU) data is critically needed. This approach provides a direct and realistic assessment of the effective inertia, which aggregates the inertia impact from SGs, loads, controlled responses of renewables/HVDC/storage, etc.

In this paper, a large disturbance measurement-based approach for estimating the US grid inertia is developed, as shown in Fig. 1. The approach makes use of real-world PMU data obtained from the Frequency Monitoring Network (FNET/GridEye) spread across the whole US. The historical field-measured PMU data has been utilized for estimating the inertia trends of the US interconnections in the past decade. This provides a quantifiable assessment of the evolution of inertia within the US over that period. The inertia evolution has been explained by the fuel mix portfolio of the US during the same period. By leveraging such real-world field data, this study offers valuable insights into the evolving dynamics of the US grid, especially in the context of increased IBRs integration and recent changes in generation mix. The outcomes of this study allow for a deeper understanding of how inertia has shifted in response to these changes and highlight key trends that are crucial for grid stability and planning. This large-scale, empirical analysis fills an important gap in the literature, offering practical insights that theoretical and simulation models alone may not be able to capture. The main contributions of this study are summarized as follows:

- The estimation of the inertia trends of the three US interconnections in the past decade using real-world PMU data collected across the whole US. In particular, the three considered US interconnections are: the Eastern Interconnection (EI), the Western Interconnection (Western Electricity Coordinating Council (WECC)), and the Texas Interconnection (Electricity Reliability Council of Texas (ERCOT)).
- A proper RoCoF time window for each US interconnection is determined to achieve an accurate and reliable estimate of the interconnection system inertia. This is performed by analyzing a statistical metric—the correlation coefficient between power mismatch and RoCoF. The selected time window is further validated through sensitivity analysis.
- The inertia trends of the three US interconnections over the past decade are analyzed and explained using the generation-by-fuel mix data. Valuable insights are extracted from such analysis.

The remainder of the paper is arranged as follows. Section II discusses the concept of inertia together with the swing equation and its general form for modern power systems. Section III explains the source of the PMU data used in this study and its preprocessing practices. Section IV describes the different factors affecting inertia estimation for an interconnection, including event start time detection and RoCoF time window selection. Section V presents the resulted inertia trends and analysis for the three US interconnections over the past decade. Finally, Section VI provides concluding remarks and potential future directions.

II. INERTIA CONCEPT AND SWING EQUATION

The kinetic energy stored in the rotating mass, such as generators and motors tied to a power system network, is defined as the inertial energy of the power system [19], [20]. The power system inertia resists any change in the speed of the SGs and thus any change in the system frequency. The kinetic energy from the spinning mass is normalized by the rated capacity of the rotating machine to obtain an inertia constant as [20]:

$$H = \frac{\frac{1}{2}J\omega_r^2}{S_r} = \frac{KE}{S_r} \tag{1}$$

where H represents the inertia constant of the machine, J is the moment of inertia of the machine, ω_r is the rotational speed, KE is the kinetic energy stored, and S_r is the rated capacity of the machine. H has the unit in seconds, representing the time it takes for the machine to provide the

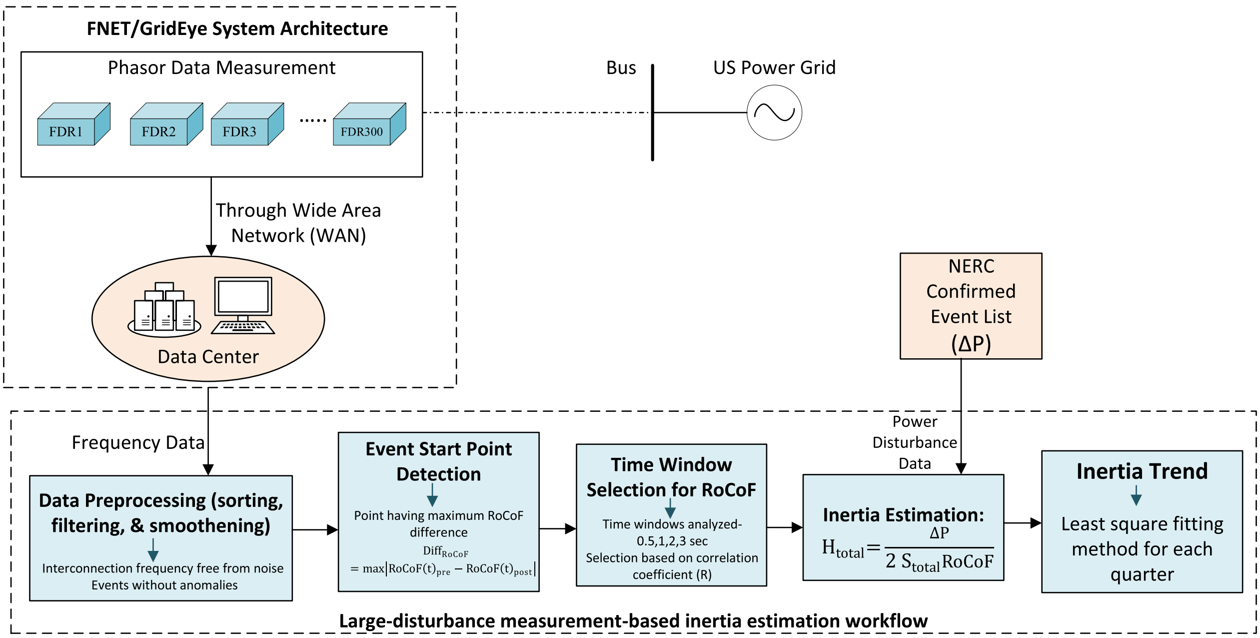

FIGURE 1. The proposed measurement-based approach for inertia estimation.

electrical energy equivalent to the stored kinetic energy in the spinning mass connected to a system, without change in mechanical input [2], [3].

A. DEFINITION OF INERTIA CONSTANT FOR CONVENTIONAL AND MODERN POWER SYSTEMS

In a conventional power grid, the total system inertia, H_{SG}, can be represented by summing the kinetic energy stored in each rotating machine, KE_i, divided by the total system capacity, S_{SG}, as [2]:

$$H_{SG} = \frac{\sum_{i=1}^{n} KE_i}{S_{SG}} = \frac{\sum_{i=1}^{n} H_i S_i}{S_{SG}} \tag{2}$$

where H_i and S_i are respectively the inertia constant and rated capacity of the ith SG, and n is the total number of SGs connected to the system.

Equation (1) can be used without any modification for the conventional power system, however, for the future or modern power grid, where IBRs are deployed in a large number, it needs a modification. Although IBRs do not have the natural frequency response characteristics, suitable inverter control strategy yields in contributing non-rotating inertia or often called as virtual inertia to the grid. So, if the virtual inertia from IBRs is considered, (2) can be modified as [3], [4], and [21]:

$$\begin{aligned} H_{total} &= \frac{\sum_{i=1}^{n} KE_i + \sum_{j=1}^{m} VIE_j}{S_{total}} \\ &= \frac{\sum_{i=1}^{n} H_i S_i + \sum_{j=1}^{m} H_j S_j}{S_{total}} \end{aligned} \tag{3}$$

$$M_{sys} = H_{total} \cdot S_{total} = \sum_{i=1}^{n} KE_i + \sum_{j=1}^{m} VIE_j \tag{4}$$

where H_{total} and S_{total} are respectively the total inertia and total capacity of the system including SGs and IBRs, H_j and S_j are respectively the virtual inertia and rated capacity of the jth IBR, VIE_j is the virtual inertial energy from the jth IBR, and m is the total number of IBRs connected to the system. The commonly expressed unit of inertia in terms of energy is MVA*s, which represents the total inertial energy of the system, denoted as M_{sys} in (4).

B. GENERAL SWING EQUATION AND FREQUENCY RESPONSE

Whenever there is a mismatch between mechanical power and electrical power due to a disturbance (difference in supply and demand), there is rotor acceleration or deceleration of SGs. The swing equation of a single machine system (considering all the SGs) that explains an electro-mechanical interplay between power disturbance and the frequency response of the system can be written as [3], [20], [22]:

$$2H_{SG}\frac{df_{pu}}{dt} = (P_m - P_e - D\Delta f_{pu}) \tag{5}$$

where $\frac{df_{pu}}{dt}$ is the RoCoF in pu, P_m is the mechanical power in pu, P_e is the electrical power in pu, D is the damping coefficient of the system, and Δf_{pu} is the change in frequency in pu. This perfectly describes the SG-dominated power system. However, as the number of IBR units having virtual inertia control gets large, the inertia can be written as in (3) and (4), and therefore, a general form of the swing equation can be written as:

$$2H_{total}\frac{df_{eq\_pu}}{dt} = (P_m - P_e - D\Delta f_{eq\_pu}) \tag{6}$$

$$H_{total} = \frac{\Delta P}{2S_{total}\frac{df_{eq}}{dt}} \cdot f_s \tag{7}$$

$$M_{sys} = H_{total} \cdot S_{total} = \frac{\Delta P}{2RoCoF} \tag{8}$$

where $\Delta P = S_{total} \cdot (P_m - P_e)$ is the power disturbance, f_{eq} is the equivalent frequency of the system consisting of SGs and IBRs, and f_s is the synchronous frequency. As the frequency deviation during the first few seconds after a disturbance is minimal, the damping term in (6) can be neglected [16], [23]. Equations (4) and (8) represent the total inertial energy of a modern power system.

To find out the total system inertia, (8) can be utilized that requires two types of data: ΔP and RoCoF. To find out the RoCoF, the inertial response after a disturbance can be used which is typically within 10 seconds (for interconnection) after the event start point [3] as shown in Fig. 2. The slope as shown in the figure gives the RoCoF. During this period, the kinetic energy stored in the spinning mass helps to negate the power loss impact. As the number of the IBRs having lack of rotating mass increases in the power system, the inertia goes down and consequently the RoCoF increases which can be justified by (8) and illustrated in Fig. 3. As in the figure, when the inertia is lowered, the frequency nadir is shifted from C to C' indicating the system is more prone to blackouts and an increase in frequency fluctuations.

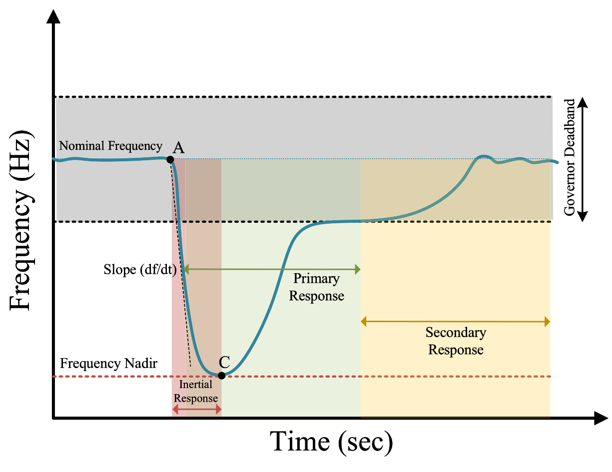

FIGURE 2. Frequency response representing the inertial, primary, and secondary responses after a large disturbance.

III. DATA COLLECTION AND FREQUENCY PREPROCESSING

A. DATA SOURCE

The frequency data is obtained via the frequency disturbance recorders (FDRs) distributed throughout the US and Canada. These PMU sensors provide continuous measurement of frequency, voltage, and phase angle from several locations throughout the US. The FNET/GridEye monitoring network,

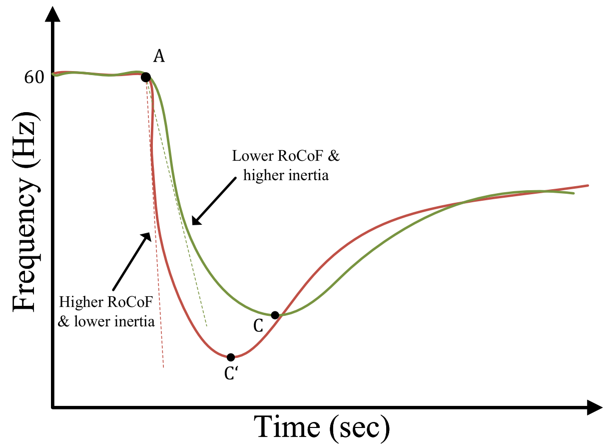

FIGURE 3. Frequency response of conventional power system (green) and future power system with high number of IBRs (red).

a synchronized network that consists of several such FDRs as shown in Fig. 4, lays a foundation for a thorough study of the different interconnections of the US. This study utilizes the historical frequency database stored in the data servers at the University of Tennessee, Knoxville (UTK) and Oak Ridge National Laboratory (ORNL) [24], [25].

This study utilizes a total of 1155 event trips that took place during the past decade (2013-2023) as shown in Table 1. The power disturbance data is obtained through the confirmed event list from the North American Electric Reliability Corporation (NERC).

TABLE 1. Number of events for each interconnection 2013-2023.

Interconnection	EI	WECC	ERCOT
No. of events utilized	356	351	448

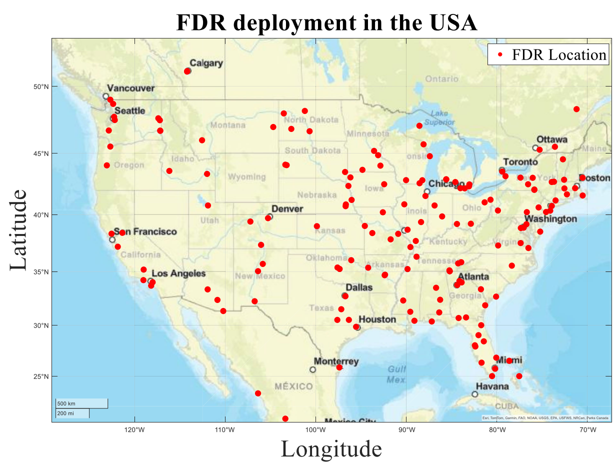

FIGURE 4. Deployment of FDRs across the US.

B. PREPROCESSING OF FREQUENCY DATA

Large power systems, such as the US Eastern and Western Interconnections, cover extensive geographical areas. These systems require numerous measurements throughout the interconnection to accurately reflect the overall frequency dynamics. Measurements taken only within a specific region might not be sufficient. They may fail to capture the complete frequency dynamics of the entire interconnection [23]. Such limited observations capture the dynamics unique to a particular area, such as oscillations and noise. However, they lack the holistic measurement needed to observe the intricacies of the whole interconnection.

For example, Fig. 5(a) shows the frequency data collected from the FDRs located throughout the Western Interconnection (in the states of WA, ID, OR, CA, CO, UT, WY, and AZ) during an event. The blue curve indicates the regional frequency dynamics particular to a region (WY) that decreases rapidly for this specific generation trip, marked by the vertical red dashed line. However, the frequencies of other regions decrease gradually. A similar case is illustrated in Fig. 5(b) for the the Eastern Interconnection, where the measurement in the state of FL has a sharp decline in frequency as compared to the other regions.

In systems with non-uniform sensor distribution, the median frequency offers a more robust estimate of system frequency as compared to the mean. In large and complex power systems, uneven sensor placement or local disturbances can introduce outliers–extreme values that distort the mean and lead to inaccurate frequency estimates. The median, by focusing on the middle value of the data, is far less sensitive to these outliers and errors. This makes the median particularly useful in large interconnections, where noise, device errors, or uneven sensor distribution are common [26]. The median frequency illustrated by the solid black line in both plots in Fig. 5 is close to the central tendency of the system frequency. This median frequency can be calculated using (9) for each timestamp.

$$f_{median} = \begin{cases} F\left[\dfrac{a+1}{2}\right] & \text{if } a \text{ is odd} \\ \dfrac{F\left[\frac{a}{2}\right] + F\left[\frac{a}{2}+1\right]}{2} & \text{if } a \text{ is even} \end{cases} \tag{9}$$

where 'a' is the number of FDRs and 'F' stands for the sorted frequency list. The resulting median frequency represents the comprehensive frequency dynamics of the interconnection.

IV. DETERMINANTS OF ROCOF AND INERTIA ESTIMATION FOR INTERCONNECTIONS

A. EVENT START POINT DETECTION

The point represented by a red color in Fig. 6, referred to as point "A", indicates the event start time. According to the NERC standard, point "A" can be determined by averaging the frequency values before the tentative event time. However, the average value may not provide an accurate RoCoF [27]. Furthermore, relying on the event time point won't give us a precise RoCoF, this is because the event time is obtained from the first FDR that records the frequency disturbance [27], while the utilized frequency for

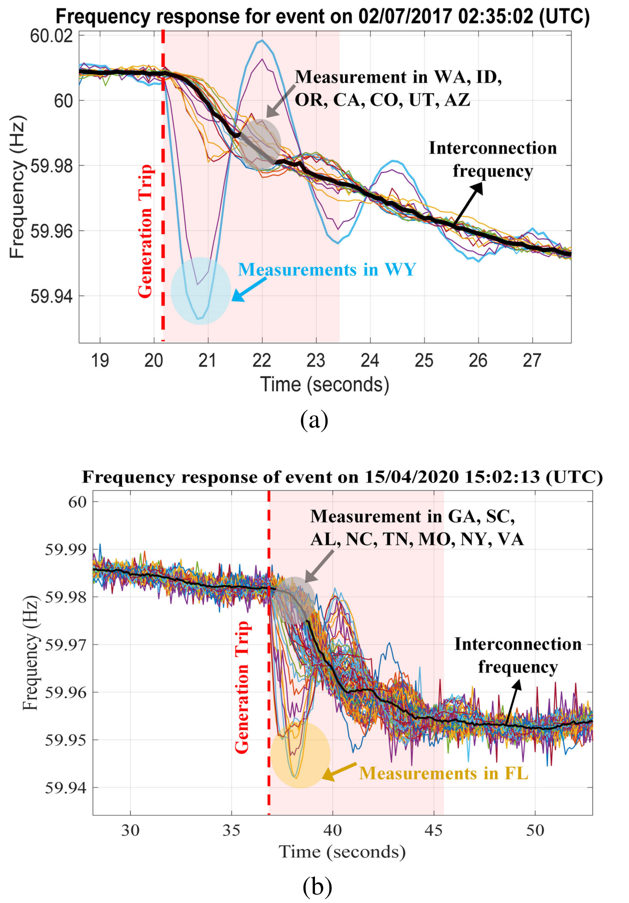

FIGURE 5. FDR measurements for two generation trip events happened in the (a) WECC and (b) EI interconnections.

the interconnection level is the median frequency. Therefore, in this study, for locating point "A" at the turning point of the median frequency when a disturbance takes place, we compute the difference between two consecutive RoCoF over time and select the maximum as follows:

$$Diff_{RoCoF} = max\left|RoCoF(t)_{pre} - RoCoF(t)_{post}\right| \tag{10}$$

where $RoCoF(t)_{pre}$ is the RoCoF computed using the frequency at time t (illustrated by the red point in Fig. 6) and the frequency at time $t - \Delta t$ (illustrated by the yellow point). Similarly, $RoCoF(t)_{post}$ is calculated using the frequency at time t and the frequency at $t + \Delta t$ (illustrated by the blue point). The point having the largest difference between pre-RoCoF and post-RoCoF is selected as point "A". This method provides the most significant change in RoCoF that represents the turning point of a frequency curve during a disturbance.

The choice of Δt determines the precision of the proposed method. The use of Δt as a tuning parameter allows the method to adjust for different interconnection systems and disturbance types. A good choice of Δt also helps to eliminate the influence of mild oscillations and noise in detecting the starting point of an event. This method computes the value of

$Diff_{RoCoF}$ for each point within a time period that starts 8-10 seconds before the event and 5 seconds after the event.

If a measurement from an FDR is extremely noisy then it is filtered out during the data preprocessing stage. Additionally, the calculated median frequency is inherently free from large noise. So, noise doesn't cause a significant problem in the event detection process. This method has been tested across diverse disturbance types, such as generation trips, pump storage shutdown events, and load shedding. It consistently identified the event start point with high accuracy. Unlike the NERC-recommended averaging approach [27], which may smooth out critical dynamics, this method captures the precise turning point of the frequency curve, thereby leading to more accurate RoCoF calculations.

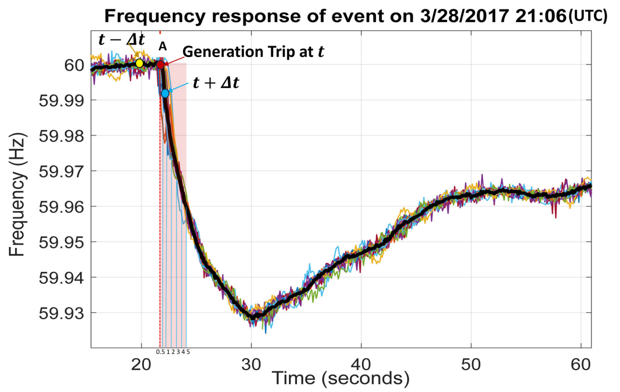

FIGURE 6. **Frequency response of an event showing RoCoF calculation at various time windows capturing inertial response.**

B. ROCOF CALCULATION

The onset time of the frequency drop recorded in each FDR correlates with the distance from the event location [28]. FDRs located near the event site experience a more rapid and pronounced frequency decline, as depicted by the frequency measurements in WY (Fig. 5(a)) and FL (Fig. 5(b)). This phenomenon is due to the time delay introduced when the inertial response is transmitted over a long distance. Inertial support travels across large geographic areas of the interconnection to reach the source of the disturbance. This causes an initial slow decrease in the median frequency that reflects the delayed arrival of inertial support.

To accurately capture regional frequency dynamics, the RoCoF should be computed in a short time frame. However, the median frequency remains largely constant until the regional frequency reaches its lowest point. As inertial support from various parts of the interconnection is integrated, the median frequency starts to decline more steadily. Because of this lag in the median frequency, using a larger time window can capture the interconnection's frequency dynamics accurately providing a better estimate for calculating RoCoF. However, excessively long time windows might unintentionally encompass the primary response from the governor. The overall network dynamics indicate a lower RoCoF during the early stages of a disturbance. In addition, a very short RoCoF time window increases noise sensitivity. Therefore, it is crucial to balance and find a trade-off between the time window size and sensitivity.

Once the event start point for the median frequency is identified as in (10), RoCoF can be calculated effectively for various time windows as:

$$RoCoF_{T_{interval}} = \frac{f_{start} - f_{start+T_{interval}}}{T_{interval}} \tag{11}$$

where f_{start} is the frequency just before the start of the event, $T_{interval}$ represents different time windows: 0.5, 1, 2, 3, 4, and 5 seconds after the start of the event as illustrated in Fig. 6.

C. TIME WINDOW SELECTION: CORRELATION COEFFICIENT AND SENSITIVITY ANALYSIS

The metric to measure the consistency in the linear relationship between an event size in megawatt (MW) and RoCoF is the correlation coefficient (R). This is also a reliability measure for the selection of the RoCoF time window. A larger value of R implies a strong linear correlation between event size in MW and RoCoF, which can help avoid capturing the primary frequency response from the governor. This ultimately leads to determining the best time window for precise RoCoF evaluation. Also, it ensures that the chosen time window captures significant dynamics without capturing unwanted noise. The R-value is determined using (12), which correlates the disturbance MW values with the RoCoF values calculated for each of the set of time windows.

$$R = \frac{1}{N-1} \sum_{i=1}^{N} \left(\frac{MW(i) - \mu_{MW}}{\sigma_{MW}} \right) \left(\frac{RoCoF(i) - \mu_{RoCoF}}{\sigma_{RoCoF}} \right) \tag{12}$$

where R represents the correlation coefficient, N denotes the number of events, MW is the vector containing the MW sizes for generation trip events, and $RoCoF$ is the vector containing the RoCoF values calculated for a specific time window. The terms μ_{MW} and μ_{RoCoF} correspond to the mean values of the MW and RoCoF vectors, respectively, while σ_{MW} and σ_{RoCoF} denote their standard deviations.

The selection of time windows for RoCoF calculation is based on the goal of capturing the system's inertial response before the onset of the primary frequency response. We observed that the correlation coefficient between RoCoF and MW begins to decrease after a certain point in time (see Fig. 7). This indicates the influence of primary frequency response, which reduces RoCoF and falsely increases the estimated inertia. Therefore, we select time windows that best reflect the inertial response while minimizing the effects of the governor's action.

The R-values, which are calculated using the RoCoF of various time windows for different years (2013 to 2023), are averaged to determine the average R-values and the corresponding standard deviation values. The results, illustrated in Fig. 7, reveal a unique pattern: the average R-value increases with the increase in the time window

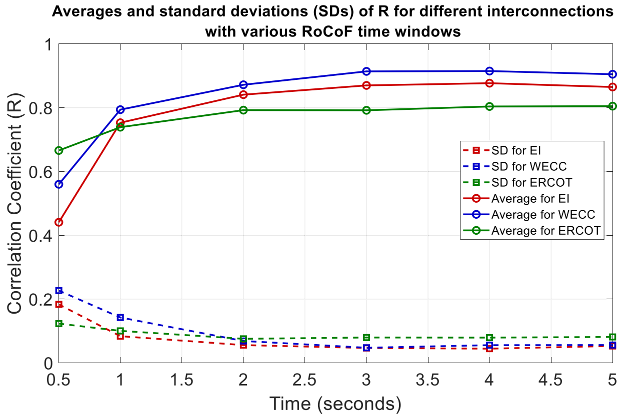

FIGURE 7. Average and standard deviation values of *R* under different RoCoF time windows for the three US interconnections.

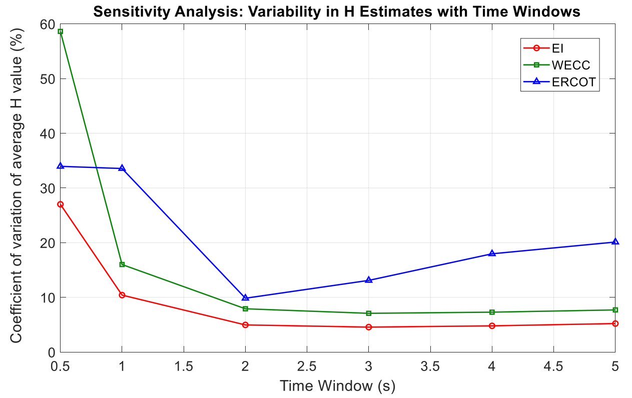

FIGURE 8. Sensitivity analysis: Variability in inertia estimates with respect to various time windows.

TABLE 2. RoCoF time window selection for the three US interconnections.

Interconnection	Time Window Selected (sec)
EI	3
WECC	3
ERCOT	2

(x-axis) to a certain point in time, while the standard deviation decreases. However, selecting a time window that is too long should be avoided since the benefit of lengthening it fades after a certain point. It also makes it prone to capture the response from the governor. For example, there is no need to select a time window beyond 3 seconds in the case of the EI. This is because the *R*-value stays almost constant once it reaches to the third second for a few time windows and then decreases. Therefore, 3 seconds is selected as the optimal time window for the RoCoF calculation in the case of the EI. Similar analysis is conducted for the other interconnections, and the selected time windows for all three interconnections are tabulated in Table 2.

In addition to using the *R*-value as a reliability metric for selecting the appropriate RoCoF time window, a sensitivity analysis is carried out to assess the variability of the inertia estimates across different time windows. The variability is represented by the coefficient of variation (CV) of average inertia values, as shown in Fig. 8. This analysis highlights the robustness of the selected time window by quantifying the consistency of inertia estimates.

From the results in Fig. 8, we can observe that the variability in inertia estimates is significantly higher at shorter time windows (e.g., 0.5s). This is primarily due to the noise sensitivity during the early stage of the event. As the time window increases, the coefficient of variation decreases sharply, reaching its minimum around 2-3 seconds for all three interconnections. Beyond 3 seconds (for EI and WECC) and 2 seconds (for ERCOT), the variability begins to increase gradually, likely due to the influence of primary frequency response. This behavior aligns with the trends observed in the *R*-values, as discussed earlier. Therefore, this sensitivity analysis confirms that the time windows chosen in Table 2 are optimal to balance precision, reduction of noise impact, and avoidance of governor action across all interconnections.

D. TYPES OF EVENTS AND OUTLIER EVENTS

Over the past decade, several events have occurred that can be categorized into different types. The first type of event can be classified as a normal generation trip, as shown in Fig. 9(a). This type of event is characterized by a sharp and distinct turning point following a disturbance, making it suitable for inertia analysis. Similarly, the second type of event that can be used for analysis is the pumped storage hydropower (PSH) turn-off events, as shown in Fig. 9(b). During the times of low power demand, PSH uses the electricity from the power grid to pump water from a lower to an upper reservoir [29]. When the pump is turned off, there is a decrease in load on the system as the pump is no longer consuming power. This event results in a positive power mismatch, causing the system frequency to increase. Consequently, PSH turn-off events can also be utilized for inertia analysis, similar to generation outage events.

Although numerous events can be used for precise inertia analysis, some events differ significantly from the two types discussed above. One such event, shown in Fig. 9(c), can be categorized as a generation trip with a rounded turning point and gradual ramping down of frequency, known as a soft trip event. This type of event poses difficulties in accurate inertia calculation. Distinguished by a staged disconnection process, the event begins with the closure of the prime mover of any type, including gas, steam, or hydro turbines. After the shutdown of the prime mover, there is a slow ramping down of the output before the actual tripping of the generator. This event typically exhibits a low RoCoF for high MW, which dramatically increases the inertia value.

Another type of event involves those with a low event starting point, as shown in Fig. 9(d), which begins below the governor's deadband. This makes them prone to capturing the primary response from the governor, which leads to unnaturally higher inertia. Other events that can cause erroneous inertia estimation include double contingencies or generation trips, which can make it difficult to detect the event start point and accurately estimate RoCoF and inertia. Such type of event is shown in Fig. 9(e).

Therefore, it is important to meticulously examine the frequency dynamics of each event and filter out those that could lead to erroneous inertia assessment. This process significantly improves the correlation coefficient between RoCoF and MW values. Removing anomalous events that deviate from established patterns significantly increases the correlation, as shown in Fig. 10. Once the outlier events are filtered out, the R-value increased from 0.81 to 0.97, demonstrating the significance of the event filtration process.

V. INERTIA CALCULATION AND ANALYSIS

For better visualization of the trend of inertia over the past decade, we have divided the total events of each year into four quarters and estimated inertia for each quarter. When visualized on a yearly graph, the inertia values can yield a true picture of the system's status during the past decade for all three interconnections and, hence, provide a comprehensive inertia assessment of the entire US power grid.

A. INERTIA EVALUATION

Utilizing the RoCoF values of specific time windows for the various interconnections, along with the power mismatch data, the systems' inertia can be computed using (8). The inertia computed using 3-second windows for the EI and WECC interconnections, and 2-second window for ERCOT, does not strictly represent the theoretical inertia. However, it provides a good estimate for illustrating inertia trends over the past eleven years. The slope of the fitted line of the MW vs. RoCoF plane in Fig. 10 provides the inertia value. To find the first-order fitted curve, whose slope indicates the inertia of each quarter, a least squares method is applied. The following describes the evaluation method:

$$2\tilde{H} = \left(RoCoF^T RoCoF\right)^{-1} \cdot RoCoF^T \cdot MW \tag{13}$$

$$\hat{M} = \left(RoCoF^T RoCoF\right)^{-1} \cdot RoCoF^T \cdot MW \cdot \frac{f_s}{2} \tag{14}$$

where

$$RoCoF = \begin{bmatrix} \frac{\Delta f_1}{\Delta t} \\ \frac{\Delta f_2}{\Delta t} \\ \vdots \\ \frac{\Delta f_b}{\Delta t} \end{bmatrix}, \quad MW = \begin{bmatrix} MW_1 \\ MW_2 \\ \vdots \\ MW_b \end{bmatrix},$$

and $\tilde{H}$ is the inertia expressed in MJ/Hz, which when multiplied by the synchronous frequency (f_s), gives us the inertia in MVA*s, represented by $\hat{M}$ in (14). The $RoCoF$ matrix contains the rate-of-change-of-frequency $\left(\frac{\Delta f_i}{\Delta t}\right)$ for all b events for a time window Δt. Similarly, the MW matrix consists of respective values of power mismatch (MW_i) for all events.

B. TREND ANALYSIS OF INERTIA

Each interconnection's inertia assessment is carried out from 2013 to 2023, as shown in Fig. 11. The green curve represents the trend of inertia for the EI, with each diamond

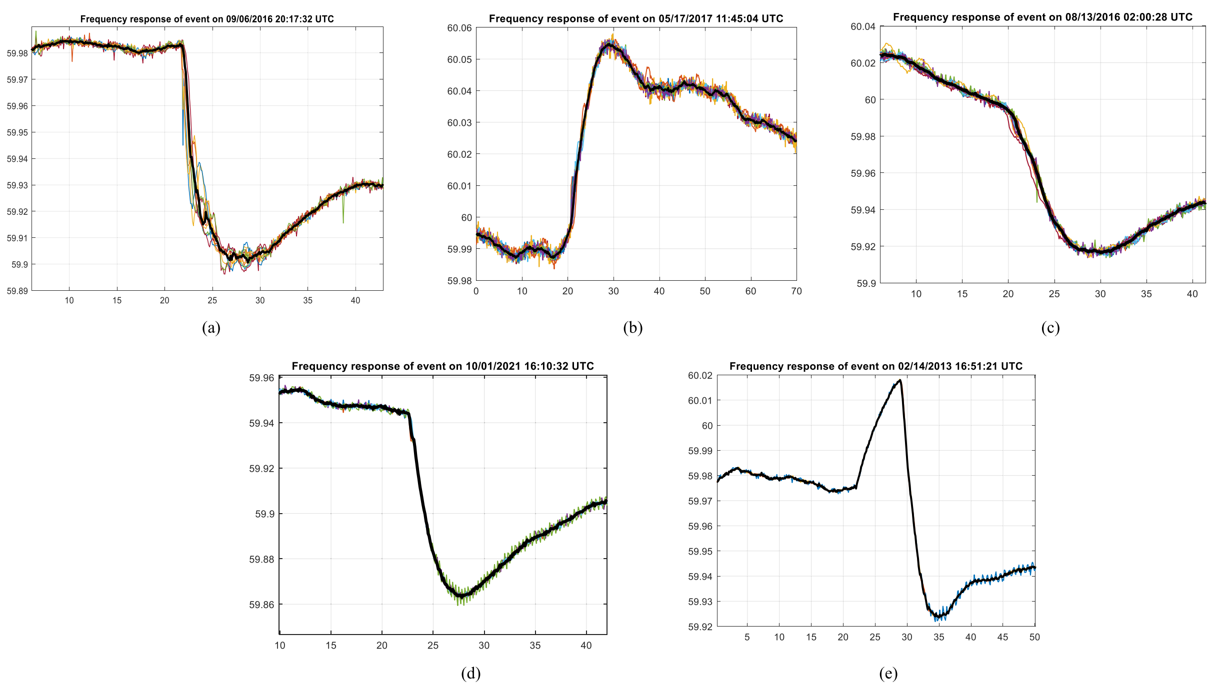

FIGURE 9. Different categories of events: (a) normal generation trip, (b) pumped storage hydropower turn-off, (c) soft generation trip, (d) event with low starting point, and (e) double events.

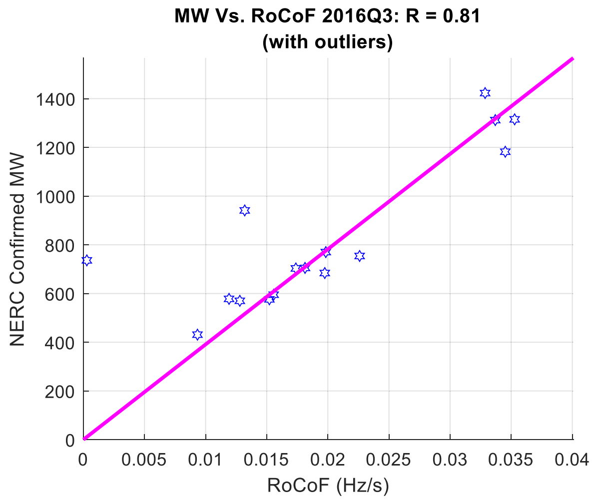

(a)

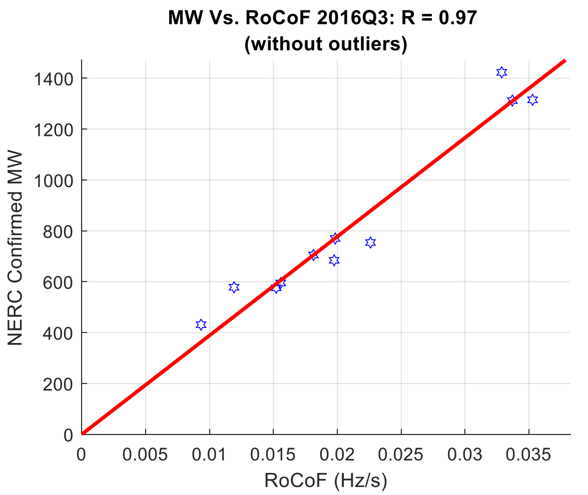

(b)

FIGURE 10. Scatter plots for event size in MW vs. RoCoF (a) with outliers and (b) without outliers.

symbol representing the quarterly inertia. There is an initial decline in inertia at the beginning, remaining fairly steady in the middle, and a slight upward trend in the past couple of years, as indicated by the green trend line in the figure (approximately 6% net decrease in inertia). Similarly, the magenta curve indicates the inertia trend for the WECC, with each dot highlighting the inertia of a quarter. We see approximately 15% net decrease in inertia for WECC during this period. Furthermore, the blue curve represents the inertia of ERCOT, connected by blue squares that indicate quarterly inertia, showing counter-intuitive results. The trend shows a slight increase in inertia over the years for ERCOT, which is in agreement with [30], as represented by the dashed blue line. The net increase in inertia for ERCOT is approximately 16% during the same period.

Inertia trends for all the three interconnections reveal a seasonal variation in inertia. It can be seen that the highest inertia values are typically obtained in the third quarter. This might be attributed to the fact that the third quarter includes the summer months, which generally have higher generator commitment patterns as compared to the other months of the year. Furthermore, the figure shows that the EI's inertia is greater than that of WECC and ERCOT. There are primarily two reasons for this: First, the EI covers a larger geographical area as compared to the other interconnections. This vast scale implies that many conventional SGs, such as natural gas and coal plants, and loads are integrated to the system, which inherently adds more to the system's inertia [31]. Second, the share of IBRs like wind and solar power is higher in WECC and ERCOT, leading to lower overall inertia as compared to the EI.

To complement the trends in Fig. 11, the box plots in Fig. 12 further validate the reliability of the inertia assessment. It illustrates the distribution of errors across years for each interconnection. The minimal variability observed in the error distributions highlights the reliability of our analysis. The stable interquartile range of error, staying close to zero throughout the period and the presence of only a few outliers further supports the robustness of the findings. This consistency adds confidence to the trends identified for EI, WECC, and ERCOT.

Different generation fuel types have unique characteristics such as startup and shutdown times, production costs, and maintenance costs, which lead to varying commitment patterns. These commitment patterns greatly impact the overall inertia of the system. Therefore, the inertia trend results in Fig. 11 can be partially explained by plotting generation by fuel type data over the past decade, obtained from the U.S. Energy Information Administration for each interconnection [7], as shown in Fig. 13. The inertia trend is slightly decreasing as expected in EI and WECC, while slightly increasing in ERCOT. This may be attributed to different variables like coal-gas generation swap, load growth, etc.

Coal, being the cheapest fuel option, is supposed to be more widely used in power generation. However, older coal units face high maintenance costs and the need to install pollution controls to comply with environmental regulations. Also, during the last decade, the price of natural gas has decreased, while the price of coal has remained consistent in the US [32]. These factors have led to coal plant retirements and an increased share of natural gas in total generation. As illustrated in Fig. 13, there is a decline in generation from coal and a corresponding increase in generation from natural gas for all three interconnections.

With this shift in energy generation, more combined cycle units—whose inertia contribution per MW might be higher as compared to coal plants depending on plants' design and type of gas engines—are being utilized. This provides a positive increase to the available inertia in the system, which has mitigated the impact of the integration of IBRs to a large extent. Although the fuel mix graph is a good tool for analyzing inertia trends, it may not effectively illustrate other factors, such as the number of generating units. Therefore,

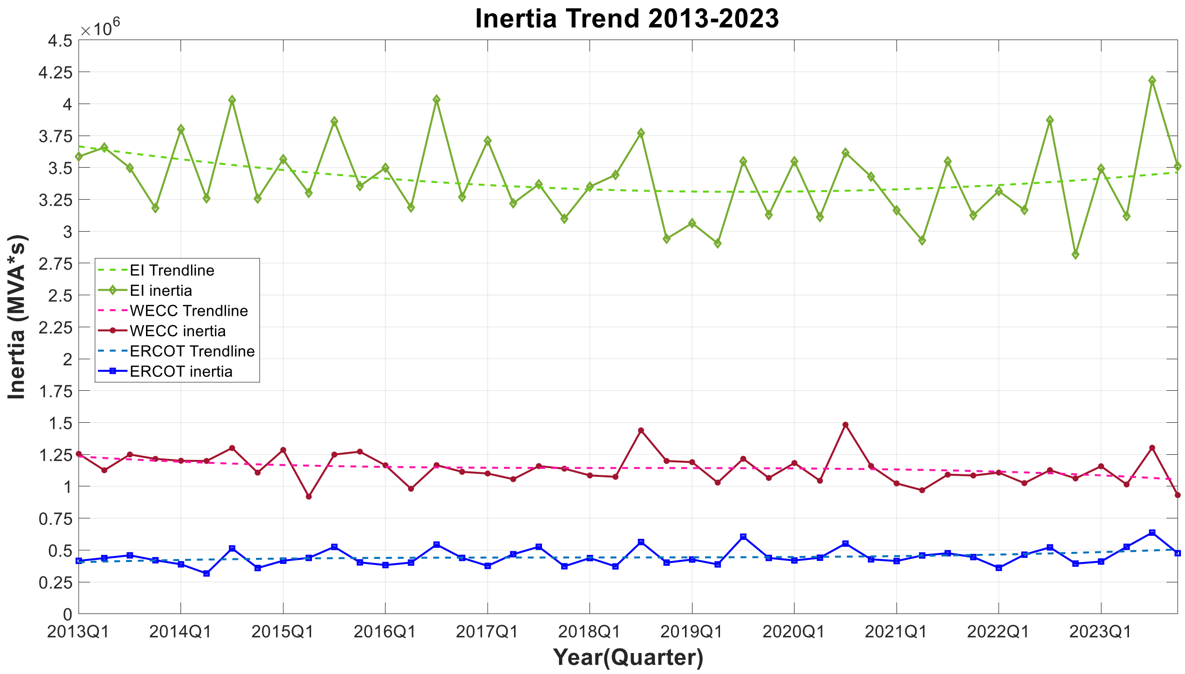

FIGURE 11. Trends of inertia for the US interconnections from 2013 to 2023.

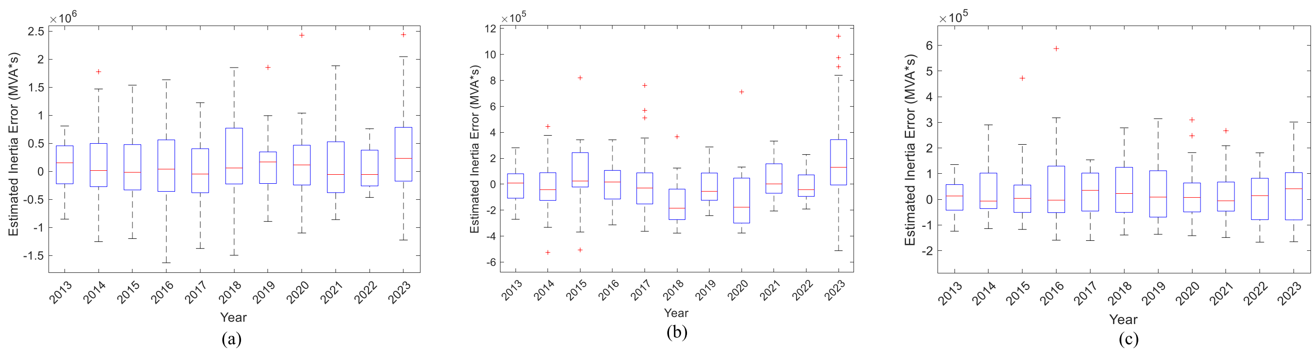

FIGURE 12. Box plots of the estimated inertia error (MVA·s) across the US interconnections from 2013 to 2023: (a) EI, (b) WECC, and (c) ERCOT. The red lines indicate median values, blue boxes represent the interquartile range, and red crosses indicate outliers.

despite the drop in generation from coal units, the retired coal units may still be operated at a lower output, contributing to the overall system inertia.

The situation within ERCOT is somewhat unique. Despite the increasing penetration of renewable energy, ERCOT has seen a counter-intuitive rise in system inertia. This is primarily due to the growth in generation capacity from both traditional and renewable sources. The system's inertia has grown due to the inclusion of more SGs, particularly those in the Private Use Network (PUN), even as the penetration of renewable energy continues to rise. PUN units, which mainly consist of combined cycle and gas steam units, have been increasing since 2014 [30]. These units add more inertia than single-cycle gas plants.

In addition to the increasing number of PUN units, ERCOT has also benefitted from the rise in gas-fired generation. This is because natural gas plants have filled the gap left by coal retirements with higher inertia contribution. Furthermore, renewable sources such as solar and wind, contrary to the concept of zero inertia, can inject/absorb active power to/from the grid, providing virtual inertia. Thanks to inverter controls; some IBRs can quickly respond to frequency fluctuations [33], [34]. However, the amount of virtual inertial support they provide is minimal, and their effectiveness in maintaining frequency remains an open question.

Nevertheless, inertia trends may also be influenced by variables other than fuel mix. It can be transmission expansion, load growth, or demand response. Transmission networks have grown as the electrical network has been developed across the US. This allows for power transfer across regions and improved access to places with high inertia. Furthermore, demand response—which shifts or reduces load to stabilize the grid—and load growth—where a rise in the demand for electricity necessitates more

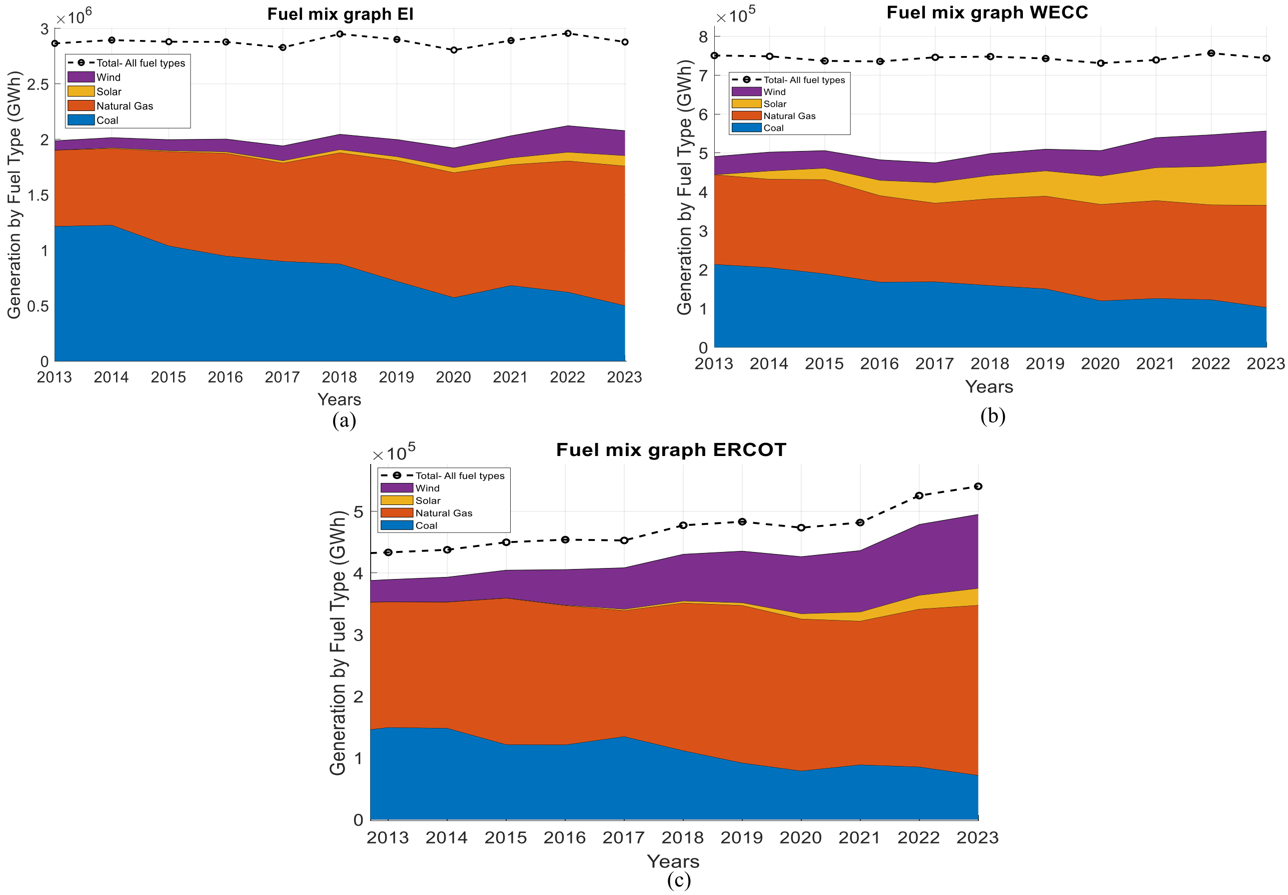

FIGURE 13. Fuel mix graph over the past decade for the (a) EI, (b) WECC, and (c) ERCOT.

synchronous generation—may alter the operational dynamics of power generation. These elements are also critical factors in how each interconnection's inertia trend is shaped.

VI. CONCLUSION

This paper presents an evaluation and analysis of inertia trends from 2013 to 2023 using historical PMU field data measured across the US, including the Eastern, Western, and Texas interconnections. To reduce noise, oscillations, and avoid regional frequency dynamics, the median frequency is utilized. Different RoCoF time windows are examined, and the time window showing a good correlation between MW and RoCoF values, with minimal primary frequency response from the governor, is chosen for each interconnection.

While the selected time window is effective in assessing the system at the interconnection level, there may be a slight amount of primary response influencing the final inertia results due to the low dead band governors near the event location. This implies that the actual values of inertia for the interconnections might be slightly lower than the obtained results. However, the impact on the results is mitigated by focusing on trend analysis and changes over time. Despite aiming to capture only the instantaneous response, emphasis is placed on capturing the broader patterns and trends of inertia over the past decade. Furthermore, validating such inertia results can be challenging, as there is no exact ground truth for system-wide inertia, especially when working with real-world data. Additionally, comparing results with dispatch-based inertia summation methods has difficulty finding time-stamped data that comprehensively covers all generators across the various interconnections.

Although the proposed methodology addresses the practical problem of investigating the inertia trends in power systems, several limitations are still present. The spatial distribution of PMUs may introduce uncertainties, as uneven placement can lead to biases in the frequency data and RoCoF used for inertia calculations. The use of the median frequency helps mitigate some of these biases, particularly in dealing with outliers and non-uniform data distribution. However, it may not fully resolve all spatial representation issues. Additionally, the inherent uncertainties in the inertia estimates, such as those arising from measurement noise or data gaps, should be considered when interpreting the results.

The future research on accurately estimating the aggregated frequencies of the interconnections using methods, such as weighted inertia approach, could be carried out for more precise inertia estimation. Additionally, different other techniques to better illustrate inertia trends can be explored. Once the number of IBRs with fast frequency response and grid-forming capabilities increases in the future, the RoCoF time window calculated for each interconnection needs to be adjusted accordingly. For the purposes of this study–focused on historical trends and large-scale interconnection behavior–the linear relationship provides a strong foundation for assessing effective inertia (composite result of generator inertia, load contributions, controlled response of renewables/HVDC/storage, etc.) over time. However, with growing IBRs, the dynamics of the power system may become more complex, and the linear model used in this paper may not fully capture these evolving interactions. So, in the future, we plan to explore more advanced models that account for the non-linearities introduced by IBRs and other emerging technologies.

ACKNOWLEDGMENT

The U.S. government retains and the publisher, by accepting the article for publication, acknowledges that U.S. government retains a nonexclusive, paid-up, irrevocable, worldwide license to publish or reproduce the published form of this manuscript, or allow others to do so, for U.S. government purposes. DOE will provide public access to these results of federally sponsored research in accordance with the DOE Public Access Plan (https://www.energy.gov/doe-public-access-plan).

REFERENCES

[1] S. Eftekharnejad, V. Vittal, G. T. Heydt, B. Keel, and J. Loehr, "Impact of increased penetration of photovoltaic generation on power systems," *IEEE Trans. Power Syst.*, vol. 28, no. 2, pp. 893–901, May 2012.

[2] F. Zeng, J. Zhang, G. Chen, Z. Wu, S. Huang, and Y. Liang, "Online estimation of power system inertia constant under normal operating conditions," *IEEE Access*, vol. 8, pp. 101426–101436, 2020.

[3] K. Prabhakar, S. K. Jain, and P. K. Padhy, "Inertia estimation in modern power system: A comprehensive review," *Electr. Power Syst. Res.*, vol. 211, Oct. 2022, Art. no. 108222.

[4] B. Tan, J. Zhao, M. Netto, V. Krishnan, V. Terzija, and Y. Zhang, "Power system inertia estimation: Review of methods and the impacts of converter-interfaced generations," *Int. J. Electr. Power Energy Syst.*, vol. 134, Jan. 2022, Art. no. 107362.

[5] ofgem. (2019). *9 August 2019 Power Outage Report*. [Online]. Available: https://www.ofgem.gov.uk/sites/default/files/docs/2020/01/9_august_2019_power_outage_report.pdf

[6] AER. (2016). *Fact Sheet: Black System Event Compliance Report: Investigation, Pre-event, System Restoration, and Market Suspension Aspects Surrounding 28 September 2016 Event*. [Online]. Available: https://www.aer.gov.au/documents/aer-black-system-event-compliance-report-investigation-pre-event-system-restoration-and-market-suspension-aspects-surrounding-28-september-2016-event

[7] EIA. *Electricity Data Browser-Net Generation for All Sectors*. Accessed: Jul. 5, 2024. [Online]. Available: https://www.eia.gov/electricity/data/browser/

[8] J. Tan, Y. Zhang, S. You, Y. Liu, and Y. Liu, "Frequency response study of U.S. Western interconnection under extra-high photovoltaic generation penetrations," in *Proc. IEEE Power Energy Soc. Gen. Meeting (PESGM)*, Aug. 2018, pp. 1–5.

[9] Y. Liu, S. You, J. Tan, Y. Zhang, and Y. Liu, "Frequency response assessment and enhancement of the U.S. power grids toward extra-high photovoltaic generation penetrations—An industry perspective," *IEEE Trans. Power Syst.*, vol. 33, no. 3, pp. 3438–3449, May 2018.

[10] WECC. (2024). *Changes in System Inertia*. [Online]. Available: https://www.wecc.org/Reliability/Changes%20in%20System%20Inertia%20(Final).pdf

[11] ERCOT. (2018). *Inertia: Basic Concepts and Impacts on the ERCOT Grid*. [Online]. Available: https://www.ercot.com/files/docs/2018/04/04/Inertia_Basic_Concepts_Impacts_On_ERCOT_v0.pdf

[12] I. Dytham. (2021). *System Inertia Monitoring National Grid ESO*. [Online]. Available: https://www.naspi.org/sites/default/files/2021-06/20210630_naspi_webinar_system_inertia.pdf

[13] K. Tuttelberg, J. Kilter, D. Wilson, and K. Uhlen, "Estimation of power system inertia from ambient wide area measurements," *IEEE Trans. Power Syst.*, vol. 33, no. 6, pp. 7249–7257, Nov. 2018.

[14] J. Zhang and H. Xu, "Online identification of power system equivalent inertia constant," *IEEE Trans. Ind. Electron.*, vol. 64, no. 10, pp. 8098–8107, Oct. 2017.

[15] P. M. Ashton, C. S. Saunders, G. A. Taylor, A. M. Carter, and M. E. Bradley, "Inertia estimation of the GB power system using synchrophasor measurements," *IEEE Trans. Power Syst.*, vol. 30, no. 2, pp. 701–709, Mar. 2014.

[16] D. P. Chassin, Z. Huang, M. K. Donnelly, C. Hassler, E. Ramirez, and C. Ray, "Estimation of WECC system inertia using observed frequency transients," *IEEE Trans. Power Syst.*, vol. 20, no. 2, pp. 1190–1192, May 2005.

[17] M. Sajjadi, H. Seifi, and H. Delkhosh, "A new approach for system-wide power system frequency model validation via measurement data," *Eng. Rep.*, vol. 4, no. 1, Jan. 2022, Art. no. e12446, doi: 10.1002/ENG2.12446.

[18] R. Sharma and G. Dhole, "Wide area measurement technology in power systems," *Proc. Technol.*, vol. 25, pp. 718–725, Jan. 2016. [Online]. Available: https://www.sciencedirect.com/science/article/pii/S2212017316305126

[19] V. Vittal, J. D. McCalley, P. M. Anderson, and A. Fouad, *Power System Control and Stability*. Hoboken, NJ, USA: Wiley, 2019.

[20] P. Kundur, "Power system stability," in *Power System Stability and Control*, vol. 10. New York, NY, USA: McGraw-Hill, 2007, pp. 1–7.

[21] P. Makolo, R. Zamora, and T.-T. Lie, "The role of inertia for grid flexibility under high penetration of variable renewables: A review of challenges and solutions," *Renew. Sustain. Energy Rev.*, vol. 147, Sep. 2021, Art. no. 111223.

[22] P. Wall, F. Gonzalez-Longatt, and V. Terzija, "Estimation of generator inertia available during a disturbance," in *Proc. IEEE Power Energy Soc. Gen. Meeting*, Jul. 2012, pp. 1–8.

[23] C. Zhang, "Measurement-based monitoring and control in power systems with high renewable penetrations," Doctoral dissertation, Dept. Elect. Eng. Comput. Sci., Univ. Tennessee, Knoxville, TN, USA, 2023.

[24] Y. Zhang, P. Markham, T. Xia, L. Chen, Y. Ye, Z. Wu, Z. Yuan, L. Wang, J. Bank, J. Burgett, R. W. Conners, and Y. Liu, "Wide-area frequency monitoring network (FNET) architecture and applications," *IEEE Trans. Smart Grid*, vol. 1, no. 2, pp. 159–167, Sep. 2010.

[25] Y. Liu, W. Yao, D. Zhou, L. Wu, S. You, H. Liu, L. Zhan, J. Zhao, H. Lu, W. Gao, and Y. Liu, "Recent developments of FNET/GridEye—A situational awareness tool for smart grid," *CSEE J. Power Energy Syst.*, vol. 2, no. 3, pp. 19–27, Sep. 2016.

[26] S. Dulal, C. Zhang, M. Baldwin, Q. Liu, M. M. Olama, N. M. Stenvig, N. Bhusal, A. Yadav, and Y. Liu, "Measurement-based approach for inertia-trend analysis of the U.S. Western interconnection," in *Proc. IEEE Kansas Power Energy Conf. (KPEC)*, Apr. 2024, pp. 1–6.

[27] Q. Liu, C. Zeng, H. Li, Z. Zhang, and Y. Liu, "Data-driven enhancement of power system disturbance magnitude estimation: Integrating two-beta and RoCoF methods," in *Proc. SoutheastCon*, Mar. 2024, pp. 799–806.

[28] S. You, Y. Liu, M. J. Till, J. Zhao, W. Yao, D. Zhou, L. Wu, Y. Su, X. Zhang, and Y. Liu, "Disturbance location determination based on electromechanical wave propagation in FNET/GridEye: A distribution-level wide-area measurement system," *IET Gener., Transmiss. Distrib.*, vol. 11, no. 18, pp. 4436–4443, Dec. 2017.

[29] EERE. *Pumped Storage Hydropower*. Accessed: Jun. 24, 2024. [Online]. Available: https://www.energy.gov/eere/water/pumped-storage-hydropower

[30] P. Du, *Renewable Energy Integration for Bulk Power Systems: ERCOT and the Texas Interconnection*. Cham, Switzerland: Springer, 2023.

[31] NREL. (2020). *Inertia and the Power Grid: A Guide Without the Spin*. [Online]. Available: https://www.nrel.gov/docs/fy20osti/73856.pdf

[32] EIA. (2024). *Monthly Energy Review*. [Online]. Available: https://www.eia.gov/totalenergy/data/monthly

[33] A. Jalali, E. Farahani, M. Delac, and N. Modi, "Impact of grid-forming inverters on frequency control of a grid with high share of inverter-based resources," in *Proc. CAIRNS Int. Symp.*, 2023, pp. 1–13.

[34] Z. Jiang, H. Yin, H. Li, Y. Liu, J. Tan, A. Hoke, B. Rockwell, and C. Kruse, "Probing-based inertia estimation method using hybrid power plants," in *Proc. IEEE Power Energy Soc. Gen. Meeting (PESGM)*, Jul. 2023, pp. 1–5.

SAURAV DULAL (Graduate Student Member, IEEE) received the B.S. degree in electrical engineering from Tribhuvan University, Pulchowk Campus, Nepal, in 2021. He is currently pursuing the Ph.D. degree with the Department of Electrical Engineering and Computer Science, University of Tennessee, Knoxville, TN, USA. His primary research interests include wide area monitoring and data analytics, low inertia power grid, and renewable energy integration.

CHENGWEN ZHANG (Member, IEEE) received the B.S. and M.S. degrees in electrical engineering from the Huazhong University of Science and Technology, China, in 2015 and 2018, respectively, and the Ph.D. degree from the Department of Electrical Engineering and Computer Science, University of Tennessee, Knoxville, TN, USA, in 2023. His research interests include microgrid operation and control, large-scale power system dynamics, data analysis, and protection.

MOHAMMED OLAMA (Senior Member, IEEE) received the B.S. and M.S. (Hons.) degrees in electrical engineering from The University of Jordan, Amman, Jordan, in 1998 and 2001, respectively, and the Ph.D. degree from the Electrical Engineering and Computer Science (EECS) Department, University of Tennessee, Knoxville, TN, USA, in 2007. He is currently a Senior Research Scientist with the Computational Sciences and Engineering Division, Oak Ridge National Laboratory, Oak Ridge, TN. He is also an Adjunct Associate Professor with the EECS Department, University of Tennessee. He has more than 180 archival publications, including journals, conference proceedings, book chapters, and technical reports in addition to numerous presentations at professional conferences and international symposia. His research interests include smart grid and smart buildings, smart grid communications and control, building-to-grid integration, renewable energy integration, wide-area monitoring and control, microgrid operation and control, cyber-physical systems, wireless communications, data analytics, statistical signal processing, and machine learning.

QIAN LIU (Graduate Student Member, IEEE) received the bachelor's degree in software engineering from The National University of Malaysia (UKM), in 2022. He is currently pursuing the Ph.D. degree in computer science with the University of Tennessee, Knoxville (UTK). His research is centered on the detection of events in power grids at the distribution level, with a specific focus on the processing and analysis of phasor measurement unit (PMU) data.

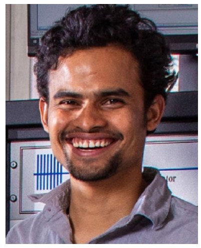

NARAYAN BHUSAL (Member, IEEE) received the B.E. degree in electrical engineering from Tribhuvan University, Pulchowk Campus, Nepal, in December 2015, the M.S. degree in electrical engineering from the University of Nevada, Las Vegas, in May 2018, and the Ph.D. degree in electrical engineering from the University of Nevada at Reno, in 2021. In May 2023, he joined Oak Ridge National Laboratory (ORNL) as a Research Scientist. Prior to joining ORNL, he was a Principal Engineer with Quanta Technology LLC. His research interests include resilience, reliability, and stability of cyber-physical energy systems; the application of machine/deep learning in power systems; virtual inertia; and community-based energy storage.

AJAY PRATAP YADAV (Member, IEEE) received the B.S. and M.S. degrees in electrical engineering from Indian Institute of Technology Roorkee and Indian Institute of Technology Kanpur, in 2010 and 2014, respectively, and the Ph.D. degree in electrical engineering from The University of Texas at Arlington, in 2021. He is currently a Research Scientist with Oak Ridge National Laboratory. His research interests include smart grids, power systems, and machine learning.

MARK BALDWIN received the B.S., M.S., and Ph.D. degrees from Virginia Tech, Blacksburg, VA, USA, in 1993, 2005, and 2008, respectively. He is currently a Principal Engineer with Dominion Generation's Fossil and Hydro Engineering Group, Glen Allen. His research interests include generating unit operation, protection, control, and modeling.

NILS STENVIG (Senior Member, IEEE) received the B.S., M.S., and Ph.D. degrees in electrical engineering from Michigan Technological University, Houghton, MI, USA, in 2008, 2010, and 2011, respectively. He is currently a Research and Development Staff Member and the Group Leader of Power Systems Resilience with Oak Ridge National Laboratory, Oak Ridge, TN, USA. His primary research interests include advanced grid modeling, interdependent energy infrastructures, and power systems reliability and resilience.

YILU LIU (Life Fellow, IEEE) received the B.S. degree in electrical engineering from Xi'an Jiaotong University, China, and the M.S. and Ph.D. degrees in electrical engineering from The Ohio State University, Columbus, OH, USA, in 1986 and 1989, respectively. She is currently the Governor's Chair with the University of Tennessee, Knoxville, TN, USA, and Oak Ridge National Laboratory (ORNL), Oak Ridge, TN, USA. She was elected as a member of the National Academy of Engineering, in 2016. She is also the Deputy Director of the DOE/NSF-Cofunded Engineering Research Center CURENT. Prior to joining UTK/ORNL, she was a Professor with Virginia Tech. She led the effort to create the North American Power Grid Frequency Monitoring Network (FNET), Virginia Tech, which is now operated with UTK and ORNL as GridEye. Her current research interests include power system wide-area monitoring and control, large interconnection-level dynamic simulations, electromagnetic transient analysis, and power transformer modeling and diagnosis.